RESEARCH ARTICLE | NOVEMBER 02 2020

# Material effects on the spallation response of metals and alloys

J. C. F. Millett; G. Whiteman; N. K. Bourne; G. D. Owen; M. Cotton; N. T. Park



*AIP Conf. Proc.* 2272, 120017 (2020)
https://doi.org/10.1063/12.0000802

# Material Effects on the Spallation Response of Metals and Alloys

J.C.F. Millett[1, a)], G. Whiteman[1)], N.K. Bourne[2)], G.D. Owen[1)], M. Cotton[1)] and N.T. Park[1)]

[1]*AWE, Aldermaston, Reading, RG7 4PR. United Kingdom.*
[2]*The University of Manchester at Harwell, Diamond Light Source, Harwell Campus, Didcot, Oxfordshire, OX11 0DE. United Kingdom.*

[a)]Corresponding author: Jeremy.millett@awe.co.uk

**Abstract.** The spall strength of materials is commonly used as a measure of a material's response to shock loading. As would be expected, this is affected by the various materials and microstructural features that control the mechanical response at all strain-rates. In this paper, we examine how the spall response varies, firstly through changes in orientation in aluminium single crystals and then at increasing levels of complexity, through age hardening in a copper-beryllium alloy, changes in Peierls stress (between niobium and molybdenum) and finally differences in unit cell (aluminium and tantalum).



## INTRODUCTION

Spallation is a process where the tensile response of a material can be probed during one dimensional shock loading. Put simply, during plate impact, release fans from the rear of the flyer and the target plates interact. Given that the regions behind the releases are reduced in pressure (in the case of unconfined rear surfaces, these pressures will be zero), where they interact, they will produce a region of net tension. Careful control of the experimental geometry can place this region in the centre of the target plate, and if this tension exceeds the tensile strength of the target material, the material can be induced to fail, and analysis of the free surface velocity trace can be used to determine the dynamic tensile (spall) strength. Like all material properties, spall strength is dependent on temperature and strain-rate, but it is also affected by additional factors such as shock stress amplitude and pulse duration, in other words, spallation is a *time integrated* process. As such, the determination of spall strength can be seen to be complex, even before microstructural factors such as grain size, phase distribution and defect content are taken into account. Finally, it should be apparent that spall strength cannot be taken in isolation as a way of characterizing the shock response of a material; the microstructural factors that affect it will also influence other features such as the Hugoniot Elastic Limit (HEL – yield strength under one dimensional strain) and shear strength. However, as long as the impact conditions and experimental geometry are kept the same, it is possible to identify the role that various microstructural features can have on the spall strength of a material. In this paper, we present the results from four studies on spallation at increasing levels of microstructural change. These are –

- Single crystalline aluminium. Here we investigate the effects of crystal orientation to the shock axis on the spall strength.
- Cu-2wt%Be-0.2wt%Co. Whilst we still remain with a single material, the effect of age hardening (creating a distribution of nanometer sized intermetallic particles throughout the microstructure) is examined.

*Shock Compression of Condensed Matter - 2019*
AIP Conf. Proc. 2272, 120017-1–120017-8; https://doi.org/10.1063/12.0000802
Published by AIP Publishing. 978-0-7354-4000-5/$30.00

- Niobium and molybdenum. Now we look at two notionally similar materials, both body centred cubic (BCC) and adjacent in the periodic table.
- Aluminium and tantalum. Finally, we examine two dissimilar (but ductile) metals where the effects of different structure (Al – FCC; face centred cubic, and Ta – BCC) and the corresponding role on plasticity.

## SINGLE CRYSTAL ALUMINIUM

In this series of experiments, three single crystals of aluminium, orientated along the three principal directions ([100], [110] and [111]) were sectioned into 6 mm thick by 40 mm diameter samples before placing them into a single target assembly, such that they could be shock loaded simultaneously. Shock stresses in the range 4 to 11 GPa were induced by the impact of 3 mm ultra pure - UP (99.999%) pure aluminium or 3.3 mm Z-cut quartz flyers in the velocity range 518 to 1246 m $s^{-1}$. Further details can be found in the paper of Owen *et al* [1].

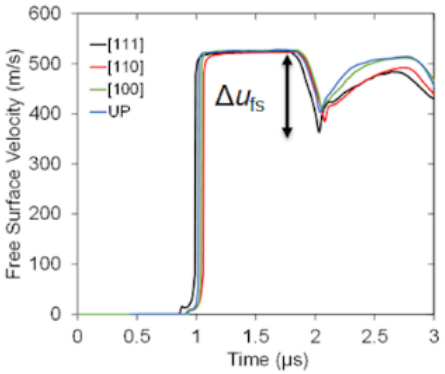


**FIGURE 1**. Free surface velocity traces for 6 mm single crystal aluminium. The flyer was 3.3 mm Z-cut quartz at 500 m $s^{-1}$.

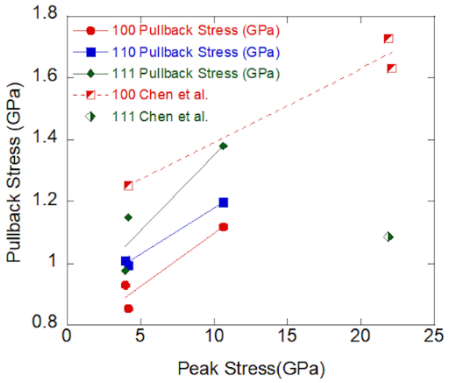


**FIGURE 2**. Spall strengths for single crystal aluminium. The previous results from Chen *et al*. [2] have been included for comparison.

The spall strength has been determined via the relation,

$$\sigma_{pullback} = \frac{\rho_0}{2} c_0 \Delta u_{fs}, \tag{1}$$

where $\rho_0$ is the density (2.699 g $cm^{-3}$), $c_0$ the zero particle velocity intercept of the shock velocity (5.33 mm $\mu s^{-1}$) [3] and $\Delta u_{fs}$ is the drop in the free surface velocity from the peak value to the first minimum, as shown in Figure 1. Note that this is a simplified version that does not take into account any stress attenuation in the spall scab. The free surface velocity traces shown in Fig. 1 are broadly similar, showing a small HEL (Hugoniot Elastic Limit), a rapid rise in plastic stress to a peak plateau before the partial release and reload that is typical of a spallation response. It can be seen that $\Delta u_{fs}$ varies according to crystal orientation, and these have been quantified using Eq. (1), and plotted as a function of the peak stress in Figure 2. Results show that [100] has the lowest spall strength, followed by [110], with the [111] orientation being the strongest. We have also included the results from an earlier investigation by Chen *et al*. [2], where it can be seen that the ordering is reversed, with [100] being stronger than [111]. The change in this sense of ordering is also shown in the spallation response of copper [4]. This is at odds with the reported quasi-static strengths of aluminium, both from our measurements [5] and those within the literature [6,7], our HEL measurements, with $HEL_{100}$=76 MPa, $HEL_{110}$=78 MPa and $HEL_{111}$=104 MPa, and similar measurements from Huang and Asay [8] $HEL_{100}$=80 MPa and $HEL_{111}$=110 MPa. From the work of Johnson *et al*. [9], the ratio of the HELs could be determined assuming that that the resolved shear stress in a FCC lattice is equal for each slip plane via the relation,

$$HEL_{111} = \frac{(C_{11}+2C_{12}+4C_{44})(C_{11}-C_{12})}{4C_{11}C_{44}} HEL_{100}, \tag{2}$$

where the elastic constants of aluminium [10] are $C_{11}$=106.8 GPa, $C_{12}$=60.4 GPa and $C_{44}$=28.3 GPa. This methodology yields a ratio of $HEL_{111}/HEL_{100}$=1.308, which compares well to our own measured ratio of 1.368 and that of Huang and Asay [8] of 1.375. Further if we apply the same analysis to copper using the appropriate values [11] of $C_{11}$, $C_{12}$ and $C_{44}$ (168.4 GPa, 121.4 GPa and 75.4 GPa respectively) this gives a ratio of 0.66 GPa, comparable to the experimentally determined value of 0.69 [12]. Although this method can only be applied to the HELs, it not only repeats the ordering of the spall strengths in aluminium, it also picks up the change in ordering in copper for both the HELs [12] and spall strength [4].

## COPPER-BERYLLIUM – AGE HARDENING

In the second series of experiments, we take a single material (in this case a Cu-2wt%Be-0.2wt%Co alloy, referred hence forth as CuBe), and manipulate its microstructure, and hence its properties by heat treatment. Two such treatments were studies; TB00 was solution treated at 790°C to yield a single phased microstructure, whilst TF00 received a further treatment at 329°C for three hours to produce a distribution of CuBe β' intermetallic particles of order 10-30 nm throughout the microstructure. Further experimental details can be found in a previous article [13]. A summary of the resultant mechanical properties (from the manufacturers) is presented in Table I.

**TABLE I**. Mechanical properties of CuBe (as supplied by the manufacturers)

| | Y (MPa) | Tensile Strength (MPa) | Elongation (%) |
|---|---|---|---|
| TB00 | 188 | 448 | 65 |
| TF00 | 1041 | 1255 | 6 |
| Copper | 50 | 200 | 50 |

As can be seen, there is an increase in yield strength of over 5 times after the aging treatment, making CuBe an excellent candidate for studying the effects of aging on the shock response (compare this to the common aluminium alloy 6061 where aging increases the yield strength by little over a factor of 2 [14]). In Figure 3, we present typical traces for CuBe, shock loaded to 5.3 GPa. Although both traces are superficially similar, clear differences are apparent. In the solution treated variant, the HEL is relatively low (although fairly well defined), followed by a rapid rise to the final shock stress. Spallation is clearly revealed by the partial release and subsequent reload. In the case of the aged material, the HEL is significantly higher (although less well defined), the rise to the final stress takes place over a longer time interval, whilst the drop to the first minimum after the peak stress is greater than in the solution treated material, indicating a significant increase in spall strength.

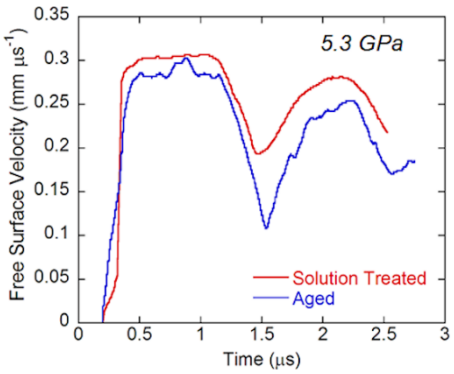


**FIGURE 3**. Free surface traces for solution treated and solution treated and aged CuBe, shocked to 5.3 GPa.

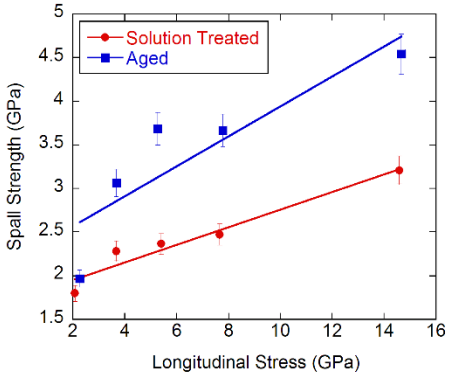


**FIGURE 4**. Spall strengths for the two heat treatments of CuBe. The straight line fits are present to aid interpretation.

Using Eq. (1), the spall strength has been quantified over the whole experimental range and the results are presented in Figure 4. Although it is clear that spall strength is significantly increased by the aging process, it is interesting to note that the level of increase (approximately x5) under quasi-static conditions is not repeated under shock loading conditions, but are at a lower level of around x2. Furthermore, similar changes in shock response have also been

observed for the HEL (0.90±.02 GPa for the solution treated material and 2.30±.06 GPa for the aged), and the shear strength (as shown in Figure 5) behind the shock front.

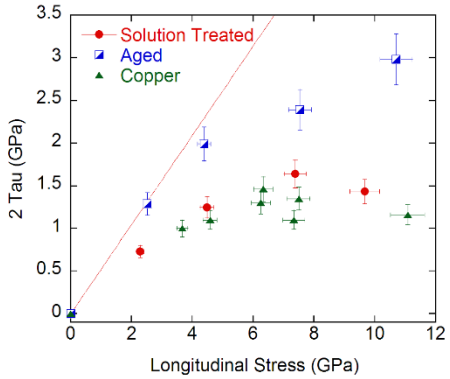


**FIGURE 5**. Shear strength versus pressure for heat treated CuBe. The straight line assumes a purely elastic response.

In a previous investigation on Al6061, the differences between the shear strengths according to heat treatment are almost non-existent. If we assume that the trends exhibited by CuBe (that is that both spall and shear strengths are increased by over a factor of two by the aging treatment) are followed by 6061, this then implies that the spall strength will also be little effected by heat treatment, although as far as we are aware, no such data has reached the open literature. The obvious approach would be to examine the shock loaded microstructures. Although this has not been done for CuBe, previous work by ourselves in Al6061 [14] showed that whilst the solution treated material responded by the formation of a dislocation cell structure, the aged microstructure consisted of a more randomized dislocation array. Further, the post shock quasi-static mechanical response showed significant hardening (compared to unshocked) as would be expected in a high stacking fault energy FCC metal such as aluminium, no such post shock hardening was observed in the aged variant. Given all these factors; the reduced strengthening of the aged material compared to solution treated, the increased plastic response time and the differences in microstructure and the reduction of post shock hardening lead us to offer the following hypothesis, in that the presence of hard, non-shearable particles within the microstructure hinder both motion and generation of dislocations, hence fewer dislocations are generated during shock loading of an aged material compared to one just solution treated. As a consequence, the high degree of shock hardening in a single phase, solution treated material allows it to effectively catch up with its aged counterpart, to the point where the increase in strength either reduces (from x5 to x2 in the case of CuBe) or even nullifies, such as occurs in 6061.

## NIOBIUM AND MOLYBDENUM – BODY CENTRED CUBIC NEIGHBOURS

The previous sections have dealt with the variation in spallation response a single material can display, either through orientation or manipulation of the microstructure. We now turn our attention to two notionally similar, but still different materials; niobium and molybdenum. These were chosen as they are both body centred cubic (BCC) and adjacent in the periodic table (niobium atomic number 41 and molybdenum 42). Therefore it would seem that these two materials should have a similar response. Further details can be found in [15]. However, it is clear from Figure 6 that these materials have very different behaviour.

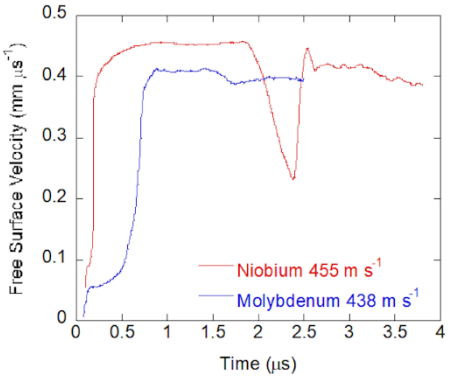


**FIGURE 6.** Free surface velocity traces for 10 mm niobium and molybdenum targets impacted with symmetrical 5 mm flyers

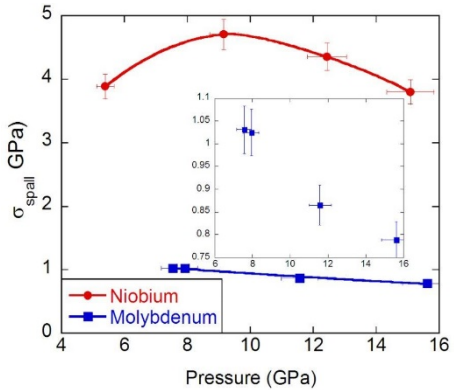


**FIGURE 7**. Spall strengths for niobium and molybdenum. The molybdenum data has been magnified in the insert.

Firstly, even though the impact geometry and velocities were near identical, the molybdenum experienced a much shorter pulse duration. This can be explained by the higher sound speed ($c_L$(Mo)=6.48 mm μs$^{-1}$ compared to $c_L$(Nb)=5.11 mm μs$^{-1}$) [3]. Further differences include a higher HEL in molybdenum (2.19 GPa compared to 1.86 GPa) and a much slower plastic rise. More pertinently, it can be seen that niobium has a much clearer defined spallation response than molybdenum, which from Eq. (1) implies a greater spall strength. This has been quantified in Figure 7 where it can be seen to be the case. Clearly these differences are linked, it would seem most likely that it is due to the shock induced deformation mechanisms. The longer rise time in molybdenum implies that the kinetics of plasticity are slower than in niobium. Murr *et al*. [16] observed dislocation densities in molybdenum in the as-received state and shocked to 15 and 25 GPa at 1.5 x $10^8$, 1.1 x $10^{10}$ and 1.2 x $10^{10}$ cm$^{-2}$, compared to nickel shocked under similar conditions [17] of $10^7$-$10^8$, 1.5 x $10^{10}$ and 16.9 x $10^{10}$ cm$^{-2}$. This is a strong indication that molybdenum accommodates the imposed shock strain mostly by the motion of dislocations already present within the microstructure rather than the rapid generation of new dislocations as does nickel. The equivalent data for niobium is more sparse, but Huang and Gray [18] indicated a dislocation density in a sample shocked to 6 GPa at 5 x $10^{10}$ cm$^{-2}$, suggesting that this material is more able to accommodate deformation via dislocation motion and generation, which in turn is controlled by the Peierls (or lattice friction) stress ($\tau_{PN}$),

$$\tau_{PN} = \frac{2G}{1-\upsilon} Exp\left(\frac{-2\pi w}{b}\right); w = \frac{a}{1-\upsilon} \tag{3}$$

where $G$ is the shear modulus, $\upsilon$ is the Poisson's ratio, $w$ is the dislocation width, $b$ is the lattice parameter and $a$ is the slip plane spacing (assumed in this case to be {110}). In Table II we present the Peierls stress for four common BCC metals [15] as well as that for the FCC nickel for comparison (the slip plane in this case is assumed to be {111}).

**TABLE II**. Peierls stress for common BCC metals. We also include the FCC nickel for comparison.

| Metal | $G$ (GPa) | $\upsilon$ | $b$ (nm) | $\tau_{PN}$ (MPa) |
|---|---|---|---|---|
| Nb | 36.3 | 0.403 | 0.330 | 70 |
| Mo | 121.5 | 0.296 | 0.315 | 629 |
| Ta | 69.0 | 0.339 | 0.331 | 252 |
| W | 160.2 | 0.279 | 0.316 | 940 |
| Ni | 81.7 | 0.315 | 0.352 | 85 |

From this, it can be seen that the Peierls stress of niobium is actually lower than nickel (known to deform by rapid dislocation generation [17]), again indicating that niobium is more likely to accommodate plasticity via dislocation generation. As a final point, we refer to the work of Swegle and Grady [19,20] where they showed that the strain-rate ($\dot{\varepsilon}$) in the plastic rise is related to the stress jump between the HEL and the final stress amplitude ($\Delta\sigma$) via the fourth power,

$$\dot{\varepsilon} = \Delta\sigma^4 \tag{4}$$

for a variety of metals, ceramics and particulate composites. We reproduce the data for a number of metals and alloys [20,21] in Figure 8.

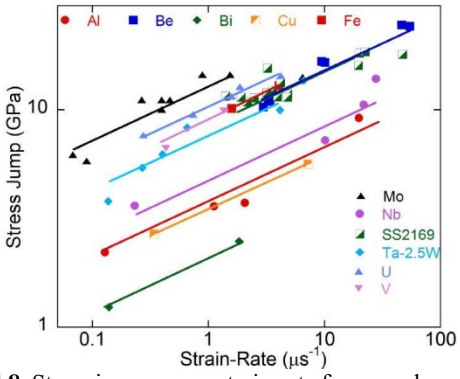


**FIGURE 8**. Stress jump versus strain-rate for a number of metals.

Although it can be seen that all materials included in this figure conform to the fourth power relation, it is also clear that they appear to arrange into two groupings (with perhaps bismuth as an outlier). Notice that niobium appears to associate with aluminium and copper (both high stacking fault FCC metals known to easily generate dislocations during shock loading), whilst molybdenum lies with materials known either to twin during shock loading (iron [22], the low stacking fault FCC stainless steel 2196 [21]), low symmetry unit cells which will again restrict dislocation generation (beryllium and uranium) or materials with a high Peierls stress such as the tantalum alloy, Ta-2.5wt%W.

## ALUMINIUM AND TANTALUM

The final comparison is now between two ductile but otherwise dissimilar metals; aluminium and tantalum. Even from representative traces presented in Figure 9, it can be seen that these materials display different behaviours.

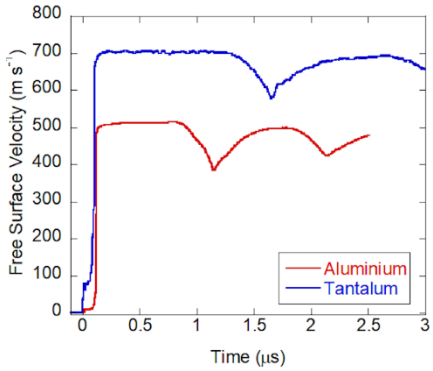


**FIGURE 9**. Typical free surface traces showing spallation in aluminium (6 mm target, 3.3 mm z-cut quartz flyer at 500 m $s^{-1}$) and tantalum (4 mm target, 3 mm tantalum flyer at 700 m $s^{-1}$).

Although both display significant spall strengths, the differences in the HEL (lower in pure aluminium) and rise time in the plastic front (lower in tantalum) suggest major differences in the mechanisms and kinetics of plasticity, which in turn will affect the spall behavior. We investigate further by plotting the variation of spall strength against pulse duration, as shown in Figure 10.

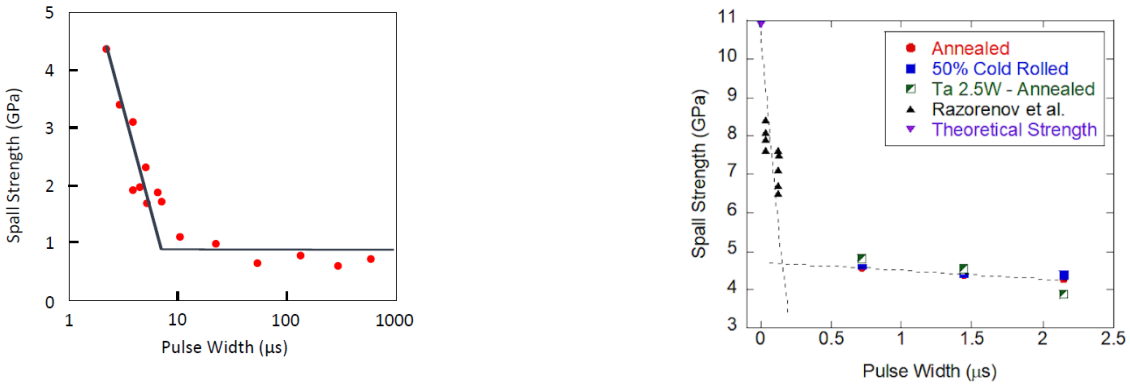


**a.** **b.**

**FIGURE 10.** Effects of pulse duration on the spall strength of a) aluminium [23] and b) tantalum [24,25].

In both plots, it can be seen that spall strength increases slightly with decreasing pulse duration, until a point whereby spall strength undergoes a significant increase in trajectory. In the case of aluminium, in collating various data, Bourne [23] pointed out this was likely to be due to a change in failure mechanism, from nucleation and growth at longer pulse durations, shifting to ductile fracture at durations below around 10 ns. Further, he went onto suggest that this short pulse duration trajectory trended towards the theoretical strength (=G/2π) as it reduced towards zero. In the case of aluminium, this would be around 4.5 GPa, which as can be seen from Fig. 10a, does appear to be the case. More recently, we repeated this exercise in tantalum, using both our own data, and the short pulse duration data of Razorenov *et al*. [25], and again we observed this trend towards the theoretical strength (this time at *ca*. 10.9 GPa). However, the duration at which this change in mechanism occurs is significantly different in these two metals. For aluminium, this change occurs at a little less than 10 ns, whilst in the case for tantalum, this occurs over an order of magnitude greater at around 150 ns. Bourne [23] has examined this further by considering the ratio of the time taken for a physical process to occur ($t_{relax}$), in this case void nucleation to the time available from the loading pulse ($t_{pulse}$),

$$F = \frac{t_{relax}}{t_{pulse}}, \tag{5}$$

therefore if the pulse duration is longer than the relaxation time of the deformation process (*i.e.* $F<1$), then that process can occur; conversely, if the opposite occurs ($F>1$), the time available is not sufficient to achieve that deformation process and as a consequence, deformation must be achieved via a different process. It is clear from Fig. 10 that the sudden increases in spall strength at reduced pulse durations are due to thus switch over where there is not enough time available for nucleation of voids, hence spallation failure is achieved by ductile failure. As pulse duration trends towards zero, it can therefore be seen spall strength would trend to the theoretical strength, as can be from Fig. 10. The differences where this time occurs between aluminium (*ca*. 10 ns) and tantalum (*ca*. 150 ns) is consistent with previous observations that the kinetics of dislocation motion and generation in FCC metals is much higher than in their BCC counterparts [23,26].

## FINAL COMMENTS

Although it is obvious that the spall strength of any material is controlled largely by the microstructure and metallurgical properties, the fact that spallation in itself is a time integrated process, and hence will be controlled in the same way that other shock induced mechanical properties are. The examples used here have shown that spall strength varies in the same way the HEL does with crystal orientation in aluminium or shear strength as a function of heat treatment in an age hardened copper-beryllium alloy. Differences in a single property such as Peierls stress can have a profound effect in otherwise similar materials such as niobium and molybdenum. Finally, the kinetics of deformation can determine whether a process can occur during the time available during shock loading, and both experimentalists and modelers should be mindful of this when ascribing mechanisms to spall experiments.

## ACKNOWLEDGMENTS

The authors would like to thank the staff of AWE plc for their help in performing these experiments.


## REFERENCES

1. G. D. Owen, D. J. Chapman, G. Whiteman, S. M. Stirk, J. C. F. Millett, and S. Johnson, J. Appl. Phys. **122,** 155102 (2017).
2. X. Chen, J. R. Asay, and S. K. Dwivedi, J. Appl. Phys. **99,** 023528 (2006).
3. S. P. Marsh, *LASL Shock Hugoniot data* (University of California Press, Los Angeles, 1980).
4. R. W. Minich, J. U. Cazamias, M. Kumar, and A. J. Schwartz, Met. Mat. Trans. A **35A,** 2663-2673 (2004).
5. J. C. F. Millett, G. T. Gray III, G. Whiteman, S. J. Fensin, and G. D. Owen, in *12th International Conference on the Mechanical and Physical Behaviour of Materials Under Dynamic Loading*, edited by E. Buzaud, A. Cosculluela, H. Couque, and E. Cadoni (EDP Sciences, Archachon, France, 2018), p. 02010.
6. J. H. Wu, W. Y. Tsai, J. C. Huang, C. H. Hsieh, and G.-R. Huang, Mater. Sci. Engng. A **662,** 296-302 (2016).
7. F. Zhang, A. F. Bower, R. K. Mishra, and K. P. Boyle, Int. J. Plas. **25,** 49-69 (2009).
8. H. Huang and J. R. Asay, J. Appl. Phys. **100** (2006).
9. J. N. Johnson, O. E. Jones, and T. E. Michaels, J. Appl. Phys. **41,** 2330-2339 (1970).
10. J. F. Thomas, Phys. Rev. **175,** 988-962 (1968).
11. W. C. Overton and J. Gaffney, Phys. Rev. **98,** 969-977 (1955).
12. O. E. Jones and J. D. Mote, J. Appl. Phys. **40,** 4920-4928 (1969).
13. J. C. F. Millett, G. Whiteman, N. T. Park, S. Case, and G. Appleby-Thomas, Acta Mater. **165,** 678-685 (2019).
14. J. C. F. Millett, N. K. Bourne, M. Q. Chu, I. P. Jones, G. T. Gray III, and G. Appleby-Thomas, J. Appl. Phys. **108,** 073502 (2010).
15. J. C. F. Millett, M. Cotton, N. K. Bourne, N. T. Park, and G. Whiteman, J. Appl. Phys. **115,** 073506 (2014).
16. L. E. Murr, O. T. Inal, and A. A. Morales, Acta Metall. **24,** 261-270 (1976).
17. F. Greulich and L. E. Murr, Mater. Sci. Engng. **39,** 81-93 (1979).
18. J. C. Huang and G. T. Gray III, Mater. Sci. Engng. **A103,** 241-255 (1988).
19. J. W. Swegle and D. E. Grady, J. Appl. Phys. **58,** 692-701 (1985).
20. D. E. Grady, J. Appl. Phys. **107,** 013506 (2010).
21. G. Whiteman, P. T. Keightley, and J. C. F. Millett, Journal of the Dynamic Behavior of Materials **2,** 337-34S6 (2016).
22. G. T. Gray III, D. B. Hayes, and R. S. Hixson, J. Phys. IV **10,** 755-760 (2000).
23. N. K. Bourne, Metall. Mater. Trans. A **42A,** 2975-2984 (2011).
24. J. C. F. Millett, G. Whiteman, N. T. Park, S. Case, and N. K. Bourne, J. Appl. Phys. **113,** 233502 (2013).
25. S. V. Razorenov, G. I. Kanel, G. V. Garkshin, and O. N. Ignatova, Phys. Solid State **54,** 790-797 (2012).
26. N. K. Bourne, G. T. Gray III, and J. C. F. Millett, J. Appl. Phys. **106,** 091301 (2009).